Electron density measurements in the National Spherical Torus Experiment detached divertor region using Stark broadening of deuterium infrared Paschen emission lines

V. A. Soukhanovskii
Lawrence Livermore National Laboratory, Livermore, California 94550

D. W. Johnson, R. Kaita, and A. L. Roquemore
Princeton Plasma Physics Laboratory, Princeton, New Jersey 08543

(Received 8 May 2006; presented on 10 May 2006; accepted 6 July 2006; published online 18 October 2006)

Spatially resolved measurements of deuterium Balmer and Paschen line emission have been performed in the divertor region of the National Spherical Torus Experiment using a commercial 0.5 m Czerny-Turner spectrometer. While the Balmer emission lines, as well as the Balmer and Paschen continua in the ultraviolet and visible regions have been extensively used for tokamak divertor plasma temperature and density measurements, the diagnostic potential of infrared Paschen lines has been largely overlooked. We analyze Stark broadening of the lines corresponding to $2-n$ and $3-m$ transitions with principal quantum numbers $n=7-12$ and $m=10-12$ using recent model microfield method calculations [C. Stehle and R. Hutcheon, Astron. Astrophys., Suppl. Ser. **140**, 93 (1999)]. Densities in the range $(5-50)\times10^{19}$ m^{-3} are obtained in the recombining inner divertor plasma in 2–6 MW neutral beam heated H-mode discharges. The measured Paschen line profiles show good sensitivity to Stark effects and low sensitivity to instrumental and Doppler broadenings. The lines are situated in the near-infrared wavelength domain, where optical signal extraction schemes for harsh nuclear environments are practically realizable and where a recombining divertor plasma is optically thin. These properties make them an attractive recombining divertor density diagnostic for a burning plasma experiment. © *2006 American Institute of Physics.* [DOI: 10.1063/1.2336456]

I. INTRODUCTION

Stark broadening of atomic hydrogen and deuterium high-n series emission lines, where n is a principle quantum number, has been used for spectroscopic measurements of plasma density in laboratory experiments and evaluation of plasma conditions in stellar atmospheres.[1] The broadening is due to the linear Stark effect in a radiating oscillator (neutral emitter) caused by the electric microfield of charged perturbers—plasma electrons and ions. In magnetically confined fusion (MCF) plasma devices divertor heat flux reduction is achieved by volume momentum and energy dissipative processes. These processes may lead to divertor plasma detachment from the target which is often accompanied by electron-ion volume recombination. Under the conditions of the detached recombining divertor plasma $T_e \leqslant 0.5-1.5$ eV and $n_e \geqslant (5-7)\times10^{19}$ m^{-3} the three-body recombination process has been identified as a principal populating mechanism of the upper levels of the deuterium Balmer ($n_{\text{lower}}=2$) and Paschen ($n_{\text{lower}}=3$) series lines.[2] We use the astrophysical notation for the series lines: for example, H10 is used for the Balmer 10-2 transition and P10 for the Paschen 10-3 transition. The corresponding ultraviolet (UV) H6–H14 and near-infrared (NIR) P8–P14 lines have been observed in many divertor MCF experiments.[3–6] While the Stark-broadened Balmer lines, as well as the Balmer and Paschen continua emissions, have been extensively used for diagnosing tokamak detached divertor plasma conditions, no application of the NIR Paschen lines has been reported. In this article we discuss electron density measurements in the detached divertor plasma region of the National Spherical Torus Experiment (NSTX) using Stark broadening of the H7–H13 and P10–P13 lines. We demonstrate the density diagnostic utility of the Paschen lines by considering the spectroscopic measurement and analysis requirements and comparing them to the Balmer line results. We find that the Paschen NIR lines show good sensitivity to Stark effects in the range $n_e \geqslant 3-5\times10^{19}$ m^{-3}, and low sensitivity to instrumental and Doppler broadenings. The P10–P13 lines are essentially free from blending with impurity ion and molecular band emission lines. These properties make the measurements an attractive recombining divertor density diagnostic of a burning plasma, such as an ITER reference operating regime—a H-mode with a partially detached divertor. The use of NIR spectroscopy for a burning plasma experiment also appears to be advantageous in respect to the signal extraction requirements. Various spectroscopic signal extraction schemes based on reflective and transmissive optics such as windows, mirrors, and fibers are presently being developed for the harsh nuclear environment. In a fusion reactor-type device the elements of a optical diagnostic signal extraction line will be routinely exposed to high energy photon, neutron, and particle fluxes. The degradation of reflective properties of metal mirrors is due to the material erosion and deposition. However, the degradation in the NIR

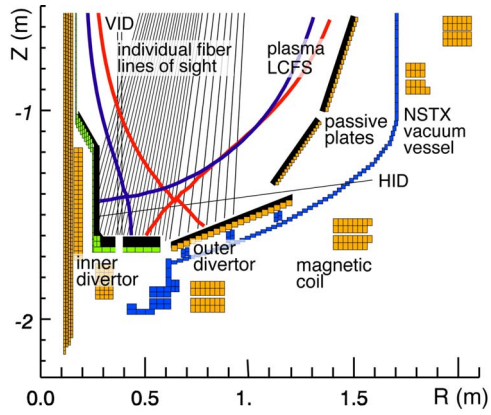

FIG. 1. Schematic of NSTX divertor multichannel spectroscopy system consisting of 32 divertor lines of sight passing through the main plasma, and the vertical and horizontal inner divertor lines of sight (labeled VID and HID). Actual spatially calibrated data are shown. Plasma last closed flux surfaces (LCFSs) of low and high triangularity and elongation shapes are also shown.

range is not as severe as in the UV and visible ranges.[7] Further, transmission properties of conventional optical fibers degrade in the intense gamma and neutron flux environments. This problem can be addressed by replacing them with hollow optical fibers. Their operation is based on the constructive interference on a layer of subwavelength holes surrounding a larger hollow core (Ref. 8 and references therein). The bandpass of the fibers is optimized for the visible and NIR light while the attenuation below 4500–5000 Å is high, making these fibers suitable for IR measurements in a burning plasma environment.

II. EXPERIMENT

The spectroscopic diagnostic arrangement is shown in Fig. 1. It comprised of an imaging lens mounted on an upper NSTX Pyrex window port with a view of the lower divertor, a 50 m long quartz fiber bundle relay optics, and a commercial spectrometer. The imaging lens was a Nikon 180 mm $f/2.8$ model Nikkor NIK18028DAF. The 32 fiber bundle included eight 1 mm core diameter fibers and twenty four 0.6 mm core diameter fibers, arranged to view the outboard and inboard divertor regions, respectively. This layout provided good spatial coverage of the strike point regions of the plasma shapes with both low and high triangularity and elongation, as shown in Fig. 1. The focusing and spatial calibration of the fiber bundle-lens system were done *in situ* by back illuminating each fiber with a He–Ne laser. When back illuminated, the fiber bundle-lens combination produced 1 cm diameter spots separated by 2 cm center-to-center distance in the inner divertor, and 1.5–2 cm diameter spots separated by 4–5 cm distance on the outboard divertor plate. Spot coordinates were measured with a computerized measuring arm with sub-millimeter precision in the vacuum vessel system of reference. For the present pilot measurements an Acton Research model Spectro-Pro 500i 0.5 m $f/6.5$ Czerny-Turner spectrometer with three input fibers was used. The spectrometer was located in a radiation-shielded room 30 m away from the NSTX test cell. An f-number matching lens system imaged fiber ends on the spectrometer entrance slit. The spectrometer was equipped with 600, 1200, and 2400 l/mm gratings and the Princeton Instruments model Spec-10:100B spectroscopic charge-coupled device (CCD) 1340×100 pixel detector. The spectrometer instrumental function was measured using the mercury lamp lines at 3650, 4047, 8516, 9115, and 9216 Å. The instrumental function was described by a Gaussian profile with the full width at half maximum (FWHM) of 1.13 Å in the UV region with the 1200 l/mm grating, and 2.30 Å in the NIR region with the 600 l/mm grating. The choice of gratings is a compromise between the spectral dispersion (resolution) and the spectral coverage in the UV and NIR regions, respectively. The photometric calibration of the spectrometer was done *in situ* with the LabSphere URS-600 radiance standard placed inside the NSTX vacuum vessel. The sensitivity rapidly decreased in the UV region, apparently due to the attenuation in the lens and fibers. Because of the optics transmission cutoff at about 3500 Å the second-order grating diffraction contribution was not an issue for the UV spectra. However, the efficiency of the 600 l/mm replica grating in the second order was found to be high, rendering the results of the NIR photometric calibration impractical, and the analysis of the P13–P15 lines difficult. An edge IR filter with a cutoff at 7200 Å was used to eliminate the second order diffraction contribution to the spectra. An *in situ* photometric calibration with the edge filter would be performed to back calibrate these spectra. The NIR spectra presented in this article were recorded without the edge filter. The P10–P12 line profiles in these spectra were affected mostly through the background contribution.

III. METHOD, RESULTS, AND DISCUSSION

A proper analysis of complex spectral features includes a rigorous collisional-radiative model for all deuterium free-bound and bound-bound transitions with ionization-recombination physics, molecular processes, radiative transfer, and line shapes. It must also account for the plasma parameter distributions and the diagnostic viewing geometry. This has been accomplished with various degrees of completeness for the Balmer line emission recorded in MCF experiments.[9–12] In Stark broadening theoretical calculations, a number of authors use the impact theory for the electron component contribution to the hydrogen line profiles, and the quasistatic approximation for the ion component contribution. Progress has been made in recent years to generalize the theory to include ion dynamic contributions, as in the model microfield method (MMM) calculations.[13] The MMM describes consistently both the line profile centers and the wings across a wide density range bridging the impact and quasistatic treatments. Although the effect of ion dynamics is not as critical for the line profiles measured under the recombining (detached) divertor plasma conditions as it is for stellar atmosphere modeling, we use the most recent MMM calculations[13] in the NSTX spectrum analysis.

While we are evaluating the analysis and modeling options for the NSTX experimental spectra, a reduced complexity analysis is used as outlined below. It addresses the experimental aspects of extracting pure Stark profiles for each line and accounting for the line blending and bremsstrahlung background contributions. We note that opacity ef-

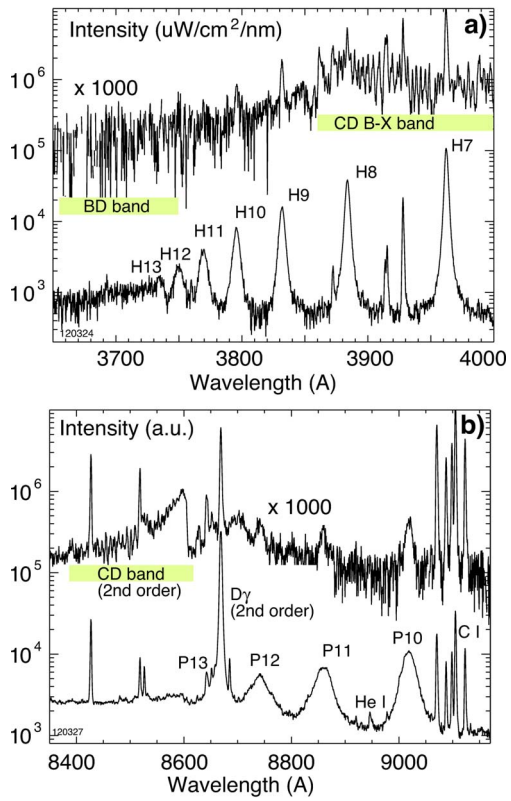

FIG. 2. Balmer (a) and Paschen (b) spectra measured in the NSTX detached divertor along the VID line of sight. The top spectra in (a) and (b) are obtained in the attached divertor phase, while the bottom spectra correspond to the detached phase.

fects under the detached divertor conditions have been found insignificant for the intensity and profile analysis of the Balmer and Paschen lines (e.g., Ref. 10). Shown in Fig. 2 are the Balmer and Paschen line spectra emitted in the inner divertor region of 4–6 MW neutral beam injection (NBI)-heated NSTX plasmas. A total profile of each line can be described by an integral convolution of Gaussian, Lorentzian, and Voigt profiles resulting from several line broadening mechanisms.[14] For the NSTX divertor plasma parameters (magnetic field $B_{\mathrm{tot}} \leqslant 0.1$ T and neutral density $n_d \leqslant 5 \times 10^{19}$ m^{-3}) the thermal and Stark broadening mechanisms are considered significant, whereas the natural broadening, van der Waals broadening, and the broadening due to the Zeeman splitting are estimated to be negligible. Accordingly, the instrumental, thermal, and Stark line profiles are considered in the total profile analysis: $\Gamma_{\mathrm{tot}}=\Gamma_{\mathrm{instr}}*\Gamma_{\mathrm{therm}}*\Gamma_{\mathrm{Stark}}$, where the convolution procedure (folding integral) is expressed by the symbol "*." A multipeak function consisting of Voigt profiles for the deuterium lines and Gaussian profiles for impurity ion lines with a polynomial background is fitted to the measured spectra using a chi-square numerical fitting procedure. We use the numerical Levenberg-Marquardt least-square minimizer MPFIT (Ref. 15) written in the IDL programming language. The fitting procedure works well for the deuterium lines with high signal-to-noise ratio; however, it can be problematic for spectra with molecular line emission contributions. The BD and CD B-X molecular band emission can be quite prominent in the divertor attached phase and during the transition to the detached phase,

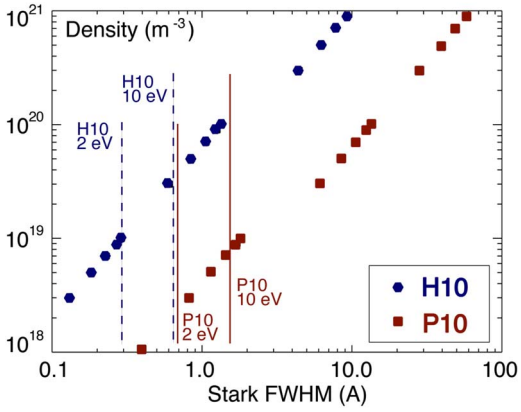

FIG. 3. Electron density as a function of Stark FWHM calculated from data in Ref. 13 for the H10 and P10 lines. Also shown are Doppler widths for $T_e=2$ and 10 eV.

as shown in Fig. 2. The line profile analysis proceeds as follows. A Voigt profile by definition is an integral convolution of a Gaussian and a Lorentzian profile. A number of numerical methods can be used to obtain a pure Stark profile from a Voigt profile fitted to experimental data. Since the Gaussian instrumental profile is measured, it would be possible to compute an integral convolution with a varying Lorentzian profile numerically until the sum of the weighted squared differences between the resulting Voigt profile and the data is minimized. To avoid a direct numerical calculation of the Voigt integral for each line, however, we adopted a different approach. Our spectral line fitting procedure uses a fast and accurate approximation of the Voigt profile.[16] To obtain a pure Stark profile the following mathematical properties of the convolution integral can be used (for example, see Refs. 14 and 17): a convolution of a Gaussian instrumental profile Γ_{instr} and a Gaussian thermal profile Γ_{therm} yields a Gaussian profile $\Gamma_{\mathrm{instr+therm}}$, whereas a convolution of a Lorentzian profile describing the Stark broadening Γ_{Stark} and the Gaussian profile $\Gamma_{\mathrm{instr-therm}}$ yields the Voigt profile Γ_{tot}. We further employ the property of a Fourier transform of the convolution integral: if $V=G*L$, then $f(V)=f(G)\times f(L)$, where f is an integral Fourier transform, and V, G, and L are the Voigt, Gaussian, and Lorentzian profiles, respectively. The deconvolution of the Gaussian and Lorentzian profiles is possible by taking an inverse Fourier transform of $f(V)/f(G)$. Thus a Stark FWHM can be extracted by fitting a Lorentzian profile to the obtained pure Stark profile. Such a rigorous deconvolution procedure may be necessary for the H7–H10 lines, where the FWHM of the convolution of the instrumental and thermal 2 eV Gaussian profiles is about 1.7 Å. However, it does not have any impact on the NIR P10–P13 line analysis: the Gaussian FWHM is about 4 Å whereas the Voigt profile FWHMs are in the range of 10–30 Å. Shown in Fig. 3 is the electron density as a function of the Stark width for the H10 and the P10 lines compiled from the tabulated results of Ref. 13. For comparison also shown are the representative 2 and 10 eV thermal linewidths. It is evident that the Paschen line profile is subject to much less uncertainties associated with the instrumental and Doppler broadening mechanisms. Its linewidth is sensitive to

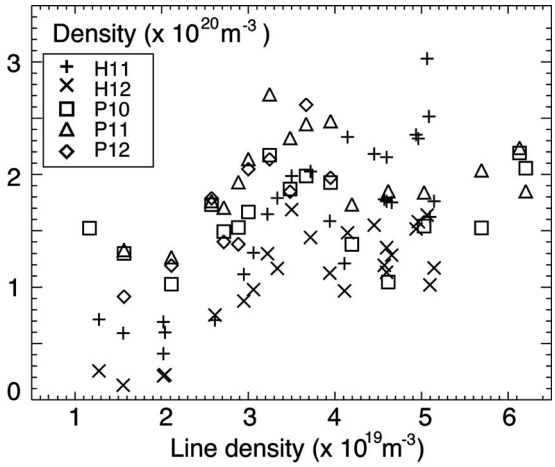

FIG. 4. Comparison of inner divertor density inferred from Balmer and Paschen lines in similar 4 MW NBI-heated plasmas as a function of main plasma line-averaged density. Error bars similar to those in Fig. 5 are not shown for clarity.

lower electron densities which are more relevant to the tokamak divertor.

Densities in the range $(5-50)\times 10^{19}$ m^{-3} have been measured in the NSTX inner divertor plasma region using the described method. The inner divertor leg is detached in NSTX throughout the operational space of NBI-heated discharges: $n_e \geqslant (2-3)\times 10^{13}$ cm^{-3} and $P_{\mathrm{NBI}} \geqslant 0.8$ MW. Strong volume recombination is evident from the spatially resolved D_γ and D_α profiles and high-n Balmer line spectroscopy.[18–20] The line emission takes place throughout the volume recombination zone, making the line-integrated spectroscopic measurement indicative of the highest n_e value in the detached divertor. Figure 4 compares the inner divertor densities inferred from the H7–H11 and P10–P13 lines in similar 1 MA, 6 MW NBI H-mode discharges. Divertor density time histories are slightly different during the lower $\bar{n}_e$ phase; however, they are essentially the same in the higher $\bar{n}_e$ phase. Shown in Fig. 5 is the time trace of the divertor density inferred from the P10–P11 lines in a high-performance 4 MW NBI H-mode plasma discharge. Despite the rise of the main plasma density throughout the discharge the inner divertor leg density remains nearly constant.

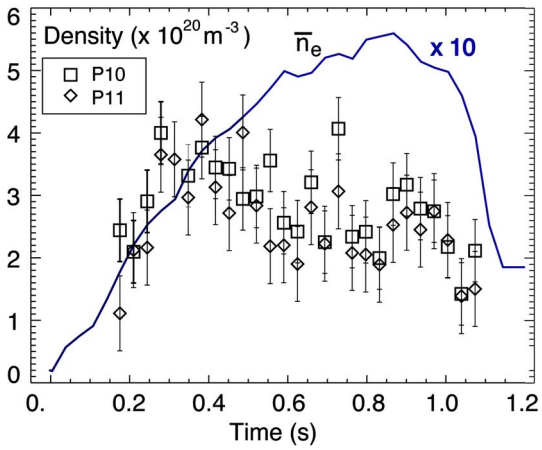

FIG. 5. Comparison of the detached divertor density inferred from the P10 and P11 lines.

In summary, we have developed a multichannel spectroscopic diagnostic and the corresponding analysis for divertor electron density measurements using Stark-broadened Balmer and Paschen emission lines originating from $n=7-13$ levels. Our pilot measurements demonstrate a good density diagnostic potential of the Paschen lines for the recombining divertor-relevant density range. The Paschen line profile measurement has a number of advantages. It is undemanding to the spectrometer resolution because of the large Stark broadening, and it is situated in the NIR spectral region, where detectors, gratings, mirrors, and relay optics have good sensitivity, reflection, and transmission properties. Future work on NSTX will focus on the comparison of the spectroscopic density measurements to divertor tile Langmuir probe measurements, an integrated spectral analysis of line shapes and intensities, and a design study of an imaging spectrometer which would take full advantage of the multichannel fiber-optic system.

ACKNOWLEDGMENTS

The authors thank Dr. R. Bell (PPPL) for useful discussions, and R. Feder, C. Priniski, D. Mastrovito, P. Roney, G. Zimmer, D. LaBrie, and T. Holoman (PPPL) for computer and technical support. The NSTX team is acknowledged for research, plasma, and neutral beam operations. This work is supported by the U.S. Department of Energy under Contract Nos. W-7405-Eng-48 at LLNL and DE-AC02-76CH03073 at PPPL.

[1] H. R. Griem, Phys. Scr., T **T83**, 142 (1999).
[2] D. Lumma, J. L. Terry, and B. Lipschultz, Phys. Plasmas **4**, 2555 (1997).
[3] J. L. Terry *et al.*, Phys. Plasmas **5**, 1759 (1998).
[4] B. Welch *et al.*, AIP Conf. Proc. **386**, 113 (1997).
[5] A. Meigs, G. McCracken, C. Maggi, R. Monk, L. Horton, M. von Hellermann, M. Stamp, and P. Breger, *Proceedings of the 27th EPS Conference on Controlled Fusion and Plasma Physics* (Budapest, Hungary, 2000), Vol. ECA 24B, pp. 1264–1267.
[6] B. L. Welch, H. R. Griem, J. Terry, C. Kurz, B. LaBombard, B. Lipschultz, E. Marmar, and G. McCracken, Phys. Plasmas **2**, 4246 (1995).
[7] A. Litnovsky *et al.*, J. Nucl. Mater. (to be published).
[8] D. Stutman *et al.*, Rev. Sci. Instrum. **76**, 023505 (2005).
[9] M. Koubiti, H. Capes, L. Godbert-Mouret, Y. Marandet, A. Meigs, S. Loch, R. Stamm, and H. Summers, AIP Conf. Proc. **645**, 67 (2002).
[10] H. A. Scott, A. S. Wan, D. E. Post, M. E. Rensink, and T. D. Rognlien, J. Nucl. Mater. **266–299**, 1247 (1999).
[11] A. Y. Pigarov, J. L. Terry, and B. Lipschultz, Plasma Phys. Controlled Fusion **40**, 2055 (1998).
[12] H. P. Summers *et al.*, Plasma Phys. Controlled Fusion **48**, 263 (2006).
[13] C. Stehle and R. Hutcheon, Astron. Astrophys., Suppl. Ser. **140**, 93 (1999).
[14] D. F. Gray, *The Observation and Analysis of Stellar Photospheres* (Cambridge University Press, Cambridge, 1992).
[15] C. Markwardt, http://cow.physics.wisc.edu/~craigm/idl/idl. html (2006).
[16] J. Humlicek, J. Quant. Spectrosc. Radiat. Transf. **27**, 437 (1982).
[17] S. G. Rautian, Sov. Phys. Usp. **66**, 245 (1958).
[18] V. Soukhanovskii *et al.*, J. Nucl. Mater. **337–339**, 475 (2005).
[19] V. Soukhanovskii *et al.*, Rev. Sci. Instrum. **74**, 2094 (2003).
[20] V. A. Soukhanovskii *et al.*, J. Nucl. Mater. (to be published).